

Near-lossless ℓ_∞ -constrained Multi-rate Image Decompression via Deep Neural Network

Xi Zhang
Shanghai Jiao Tong University
zhangxi_19930818@sjtu.edu.cn

Xiaolin Wu
Shanghai Jiao Tong University
McMaster University
xwu510@gmail.com

Abstract

Recently a number of CNN-based techniques were proposed to remove image compression artifacts. As in other restoration applications, these techniques all learn a mapping from decompressed patches to the original counterparts under the ubiquitous ℓ_2 metric. However, this approach is incapable of restoring distinctive image details which may be statistical outliers but have high semantic importance (e.g., tiny lesions in medical images). To overcome this weakness, we propose to incorporate an ℓ_∞ fidelity criterion in the design of neural network so that no small, distinctive structures of the original image can be dropped or distorted. Moreover, our anti-artifacts neural network is designed to work on a range of compression bit rates, rather than a fixed one as in the past. Experimental results demonstrate that the proposed method outperforms the state-of-the-art methods in ℓ_∞ error metric and perceptual quality, while being competitive in ℓ_2 error metric as well. It can restore subtle image details that are otherwise destroyed or missed by other algorithms. Our research suggests a new machine learning paradigm of ultra high fidelity image compression that is ideally suited for applications in medicine, space, and sciences.

1. Introduction

In many professional applications of computer vision, such as medicine, remote sensing, sciences and precision engineering, high spatial and spectral resolutions of images are always of paramount importance. As the achievable resolutions of modern imaging technologies steadily increase, users are inundated by the resulting astronomical amount of image data. For example, a single pathology image generated by digital pathology slide scanner can easily reach the size of 1GB or larger. For the sake of operability and cost-effectiveness, images have to be compressed for storage and communication in practical systems.

Unlike in consumer applications, such as smartphones and social media, where users are mostly interested in image esthetics, professionals of many technical fields are more concerned with the fidelity of decompressed images. Ideally, they want mathematically lossless image compression, that is, the compression is an invertible coding scheme that can decode back to the original image, bit for bit identical. Although the mathematically lossless image coding is the ultimate gold standard, its compression performance is too limited. Despite years of research [31, 5, 21, 3], typical lossless compression ratios for medical and remote sensing images are only around 2:1, which fall far short of the requirements of most imaging and vision systems.

Due to the above difficulty, many users are forced to adopt a lossy image compression alternative, such as JPEG or JPEG 2000. Instead of aggressive compression as in consumer applications, professional users (e.g., doctors, scientists and engineers) set very high quality factors in lossy compression to keep compression distortions at minimum. However, strictly speaking, short of lossless coding, compression noises are inevitable; thus if and how compression noises can be removed after the decompression is a challenging and worthy research problem. Recently, a number of machine learning-techniques are proposed to polish the decompressed images via a learnt mapping from decompressed image patches to their original counterparts [10, 12, 15].

Apparently still being motivated by consumer applications, the above said mappings are learnt using training data under the ubiquitous ℓ_2 metric. This approach is incapable of restoring distinct image details lost in the compression process, which are statistical outliers but nevertheless vital to image semantics. Such cases are common in machine vision applications; for examples, one is searching in a big ocean for a small boat, or a small lesion in a large organ. An ℓ_2 -based algorithm is prone to override such small structures by whatever dominant patterns in the background: ocean waves in the first example and liver textures in the second example.

In order to overcome the above identified drawback of existing techniques, we propose to incorporate an ℓ_∞ fidelity criterion in the design of a CNN for the task of compression noise removal. The novelty is to impose a tight error bound on each single pixel so that no small structures of the original image can be dropped or distorted. To achieve this design objective, we require the compression to be conducted in collaboration with the proposed CNN-based decompression. Fortunately, the so-called near-lossless image compression methods [17, 2, 7, 30], which were developed for demanding high-fidelity applications of machine vision, suit our purpose perfectly.

The main technical development of this work is to build a deep neural network G to learn a mapping from the ℓ_∞ -encoded images to the corresponding latent images. In existing CNN-based methods for removing compression artifacts, MSE loss, perceptual loss and adversarial loss were combined, aiming at high perceptual quality. However, for our purpose of faithfully reconstructing the latent image on a pixel-by-pixel basis, we drop the perceptual loss in the design of our anti-artifacts CNN. More critically, we are vigilant about the side effects of the MSE loss and the adversarial loss. The former criterion, due to the nature of ℓ_2 metric, tends to smooth out subtle small image features; the latter criterion can fabricate false features. These distortions, which are detrimental and should be prevented at all costs in the professional fields of medicine, space, engineering and sciences, can be suppressed by adding an ℓ_∞ fidelity term in the optimization of network G as proposed above. The resulting neural network G is called ℓ_∞ -CNN in the sequel. Moreover, unlike the previous CNN-based methods for artifacts removal that are designed for a fixed compression bit rate (JPEG quality factor), the new ℓ_∞ -CNN is made universal in terms of bit rates.

The above outlined ℓ_∞ -CNN decompressor in conjunction with a collaborative ℓ_∞ -constrained compressor presents a new paradigm of ultra high fidelity image compression. Through extensive experiments, we demonstrate that the proposed new paradigm outperforms the state-of-the-art image compression systems in ℓ_∞ metric and perceptual quality for a given compression ratio, while being competitive in ℓ_2 error metric as well.

The remainder of this paper is structured as follows. Section 2 reviews the existing works for compression artifacts removal, and introduces the framework of near-lossless image coding concisely. Section 3 describes how to incorporate the proposed ℓ_∞ fidelity term into the optimization of our neural network. In section 4, we conduct experiments to evaluate the effectiveness of the proposed ℓ_∞ -constrained artifacts removal algorithm. In section 5, we compare our results with the state-of-the-art methods on a set of aerial and satellite images and three commonly used datasets. Section 6 concludes the paper.

2. Related Works

2.1. Compression Artifacts Removal

There is a rich body of literature on techniques for removing compression artifacts in images [11, 33, 19, 6, 8, 10, 15]. The majority of the studies on the subject focus on postprocessing JPEG images to alleviate compression noises, apparently because JPEG is the most widely used lossy compression method. The published works can be classified into two categories: explicit model-based methods and data-driven learning-based methods.

In the first category, Reeve *et al.* [24] proposed to remove structured discontinuities of DCT code blocks by Gaussian filtering of the pixels around the DCT block boundaries. This work was improved by Zhai *et al.* [32] who performed postfiltering in shifted overlapped windows and fused the filtering results. A total minimum variation method constrained by the JPEG quantization intervals was used by Alter *et al.* [1] to reduce blocking artifacts and Gibbs phenomenon while preserving sharp edges. Bredies *et al.* [4] studied optimality conditions of the TV minimization approach in infinite dimension, and used a primal-dual algorithm to solve a discrete version. Zhang *et al.* [33] approached the problem by merging two predictions of DCT coefficients in each block: one prediction is derived from nonlocal blocks of DCT coefficients and the other from quantized values of DCT coefficients. Foi *et al.* [11] proposed to use attenuated DCT coefficients to estimate the local image signal under an adaptive shape support.

In the class of data-driven learning-based methods, an early approach is sparse coding. Chang *et al.* [6] proposed to use a sparse dictionary learnt from a training image set to remove the block artifacts. Liu *et al.* proposed a dual-dictionary method [20] carried out jointly in the DCT and pixel domains. Given the recent rapid development of deep convolutional neural networks (CNN), a number of CNN-based compression artifacts removal methods were published [10, 28, 15, 12]. Borrowing the CNN for super-resolution (SRCNN), Dong *et al.* [10] proposed an artifact reduction CNN (ARCNN). The ARCNN has a three-layer structure: a feature extraction layer, a feature enhancement layer, and a reconstruction layer. This CNN structure is designed in the principle of sparse coding. It was improved by Svoboda *et al.* [28] who combined residual learning and symmetric weight initialization. Recently, Guo *et al.* [15] and Galteri *et al.* [12] proposed to reduce compression artifacts by Generative Adversarial Network (GAN), as GAN is able to generate sharper image details. It should be noted, however, that the GAN results may fabricate a lot of false hallucinated details, which is strictly forbidden in many scientific and medical applications.

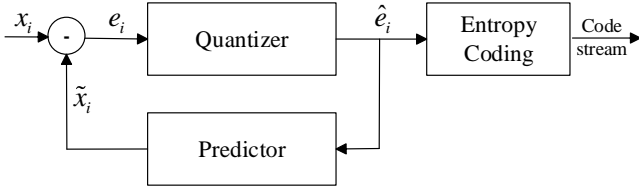


Figure 1. The illustration of predictive coding framework.

2.2. Near-lossless Image Coding

In the compression literature, near-lossless image coding refers to the ℓ_∞ -constrained compression schemes that guarantee the compression error to be no larger than a user-specified bound for every pixel. This can be realized within the framework of classic predictive coding as illustrated in Figure 1. Denoting by X an image and x_i the value of pixel i , image X is compressed pixel by pixel sequentially, by first making a prediction of x_i :

$$\tilde{x}_i = F(C_i) \quad (1)$$

where C_i is a causal context that consists of previously coded pixels adjacent to x_i , and then entropy encoding and transmitting the prediction residual

$$e_i = x_i - \tilde{x}_i. \quad (2)$$

At the decoder side, x_i is recovered without any loss as $e_i + \tilde{x}_i$. However, to gain higher compression ratio, one can quantize e_i uniformly in step size τ to

$$\hat{e}_i = \begin{cases} (2\tau + 1) \lfloor (e_i + \tau)/(2\tau + 1) \rfloor & e_i \geq 0 \\ (2\tau + 1) \lfloor (e_i - \tau)/(2\tau + 1) \rfloor & e_i < 0 \end{cases} \quad (3)$$

In this way, the decoded pixel value becomes $y_i = \hat{e}_i + \tilde{x}_i$, with quantization error

$$\begin{aligned} d &= x_i - y_i \\ &= (e_i + \tilde{x}_i) - (\hat{e}_i + \tilde{x}_i) \\ &= e_i - \hat{e}_i \end{aligned} \quad (4)$$

But by Eq(3), the quantization error will be no greater than the bound τ for every pixel:

$$-\tau \leq x_i - y_i \leq \tau \quad (5)$$

The above inequalities not only impose an ℓ_∞ error bound, but more importantly they, for the purpose of this work, provide highly effective priors, on per pixel, to optimize the deep neural networks for compression artifacts removal.

3. Methodology

3.1. Problem Formulation

Inheriting the symbols introduced above, X denotes the original image, $Y = A^{-1}A(X)$ the decompression result of compressing X by a near-lossless compression algorithm A . In the restoration of decompressed image Y , the aim is to compute a refined reconstruction image \hat{X} from a decompressed image Y by maximally removing compression artifacts in Y .

To solve the problem of compression artifacts removal, we train a neural network ℓ_∞ -CNN (denoted by G) that takes decompressed image Y as its input and returns the restored image $\hat{X} = G(Y)$. In order to satisfy the stringent fidelity requirements of medical and scientific applications, the final output image \hat{X} needs to be close not only perceptually but also mathematically to the original image X . Having this design objective in mind, we optimize the ℓ_∞ -CNN with a new cost function $L_G(X, G(Y))$:

$$G = \arg \min_G \sum_{n=1}^N L_G(X_n, G(Y_n)), \quad (6)$$

for a given training set containing N samples $\{(X_n; Y_n)\}_{1 \leq n \leq N}$. Compared with existing works, the new cost function L_G , to be discussed in detail in subsection 3.3, adds an ℓ_∞ error bound in the reconstruction process.

3.2. Network Architecture

Considering that an original image and its decompressed version populate on different manifolds, we propose to use a generative adversarial network (GAN) [13, 22, 23, 9, 34] to perform the task of compression artifacts removal. For our task, one of image restoration, network ℓ_∞ -CNN outlined above, as the generator, is tuned to pass the test of a discriminative network D . The latter network is trained to distinguish the output results of the former network from original images.

Recent works show that deeper neural network architectures [26, 29] can achieve superior results, as they have sufficient capacity to learn a mapping with very high complexity. In addition, networks designed with residual units containing skip connections [16] have achieved the state-of-the-art results for many high-level vision tasks like recognition, segmentation and low-level vision tasks like super-resolution, etc. Built upon the past successes of others, we adopt the residual units in the construction of our deep neural network ℓ_∞ -CNN for near-lossless ℓ_∞ -constrained image decompression. Like in SRGAN [18], our generative network ℓ_∞ -CNN contains 16 residual units. Each residual unit consists of two convolutional layers with small 3×3 kernels and 64 feature maps, followed by batch-

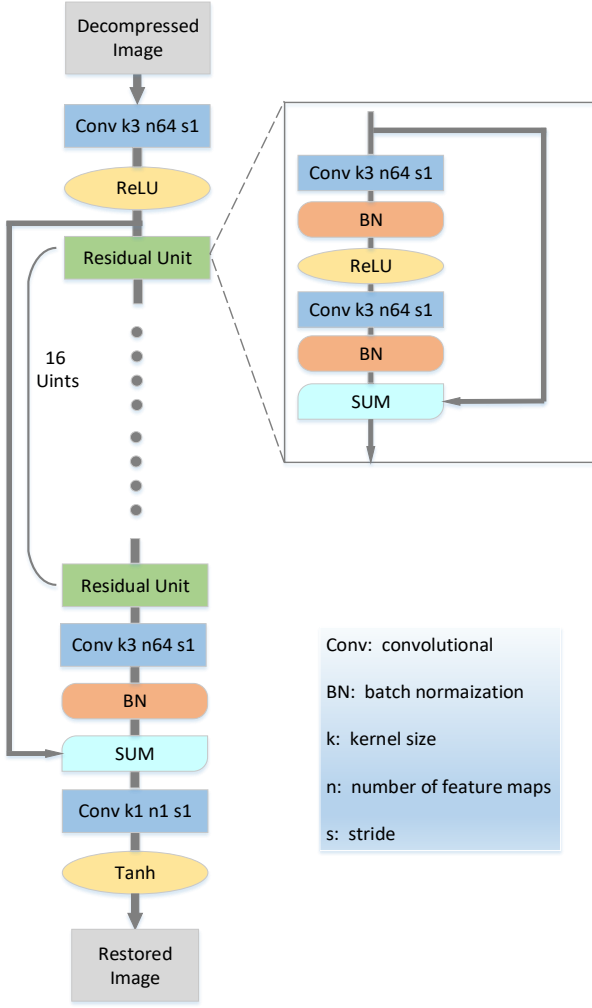


Figure 2. The architecture of our generative network ℓ_∞ -CNN.

normalization layers and ReLU activation layers. The integral architecture of network ℓ_∞ -CNN is illustrated in Figure 2. The discriminative network D will be introduced in subsection 3.3.2.

3.3. Loss Function

In this section, we will discuss the proposed loss function L_G in detail. Generally, L_G consists of three parts: MSE loss, adversarial loss and ℓ_∞ -constrained loss. The three loss functions are adopted to jointly optimize the proposed ℓ_∞ -CNN.

3.3.1 MSE loss

The Mean Squared Error (MSE) loss is defined as:

$$L_{mse} = \frac{1}{WH} \sum_i (\hat{x}_i - x_i)^2 \quad (7)$$

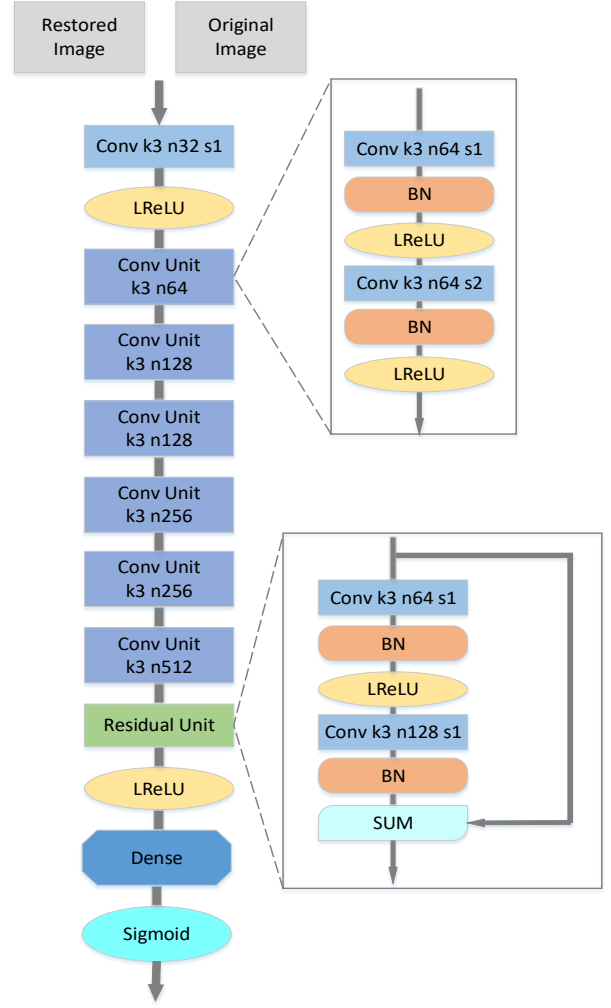


Figure 3. The architecture of our discriminative network D .

where x_i and \hat{x}_i are the values of the i -th pixel in X and \hat{X} , W and H are the width and height of X . Although MSE loss is the most widely used loss function in image restoration algorithms, it has been criticized for producing overly smooth results. Solely minimizing MSE seeks a good approximation in average sense, but it takes the risk of destroying distinctive image details which may be statistical outliers but have high semantic importance.

3.3.2 Adversarial loss

Following Goodfellow *et al.*'s wisdom, we define a discriminative network D optimized along with the proposed ℓ_∞ -CNN to solve the following min-max problem:

$$\min_G \max_D V(G, D) = \mathbb{E}_X [\log D(X)] + \mathbb{E}_Y [\log(1 - D(G(Y)))] \quad (8)$$

In practice, for better gradient behavior, we minimize $-\log D(G(Y))$ instead of $\log(1 - D(G(Y)))$, as proposed in [13]. Therefore, the adversarial loss for training generative network ℓ_∞ -CNN is defined as:

$$L_{adv} = -\log D(G(Y)) \quad (9)$$

and the loss for optimizing discriminative network D is defined as:

$$L_D = -[\log(D(X)) + \log(1 - D(G(Y)))] \quad (10)$$

In our task, minimizing L_{adv} forces the generative network ℓ_∞ -CNN to produce restored images that cannot be distinguished from the original images by D . Meanwhile, minimizing L_D forces the discriminative network D to distinguish whether an image is original image or the restored image produced by ℓ_∞ -CNN.

The architecture of our discriminative network D is improved on the discriminator of SRGAN [18]. Specifically, we deepen the network and add a residual unit before the dense layer. As shown in Figure 3, the discriminator D contains six convolutional units and a residual unit. Each convolutional unit consists of two convolutional layers, respectively followed by a batch-normalization layer and a LeakyReLU activation layer. The newly added residual unit contains two convolutional layers, and each of them is followed by a batch-normalization layer. For LeakyReLU, the slope of the leak is set to 0.2.

However, as demonstrated in [18, 15, 12], adversarial training may produce some fake image constructs just for the sake of perceptual quality. But as we stressed in the introduction and for obvious reasons, such fake constructs are absolutely forbidden in scientific and medical applications.

3.3.3 ℓ_∞ -constrained loss

To overcome the above identified weaknesses of MSE loss and adversarial training, we incorporate the ℓ_∞ fidelity criterion of near-lossless compression into the optimization of ℓ_∞ -CNN. The strict error bound restriction will force ℓ_∞ -CNN to produce reconstructed results with restored small structures and less hallucinated details.

Given the error bound τ of near-lossless compression algorithm and the decompressed image Y , according to Eq(5), the reconstructed image \hat{X} should satisfy the following constraint:

$$y_i - \tau \leq \hat{x}_i \leq y_i + \tau \quad (11)$$

where i traverse all pixels in \hat{X} and Y .

For pixels in \hat{X} , the ℓ_∞ -constrained loss penalizes the pixel values that are out of the range $[y_i - \tau, y_i + \tau]$, but does not affect those that are in the range $[y_i - \tau, y_i + \tau]$.

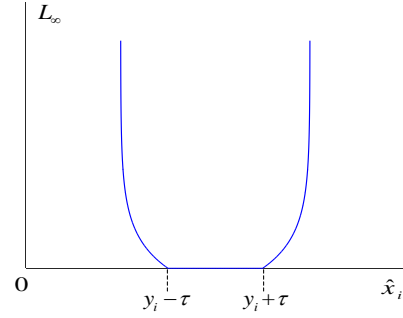


Figure 4. The illustration of ℓ_∞ -constrained loss L_∞ .

For this goal, we rewrite the Eq(11) as:

$$|\hat{x}_i - y_i| \leq \tau \quad (12)$$

and formulate the elaborate ℓ_∞ -constrained loss as following:

$$L_\infty = -\frac{1}{WH} \sum_i \log[1 - \max(|\hat{x}_i - y_i| - \tau, 0)] \quad (13)$$

As illustrated in Figure 4, the ℓ_∞ -constrained loss will increase rapidly when pixel values are out of range $[y_i - \tau, y_i + \tau]$. This severe penalty can force ℓ_∞ -CNN to produce results satisfying ℓ_∞ constraint.

3.3.4 Joint optimization

We combine the aforementioned three loss functions to jointly optimize the proposed ℓ_∞ -CNN. The joint loss function is defined as:

$$L_G = L_{mse} + \lambda_1 L_{adv} + \lambda_2 L_\infty \quad (14)$$

where λ_1 and λ_2 are hyper-parameters.

In the training phase, we alternate between one step of optimizing ℓ_∞ -CNN and one step of optimizing D , following the instructions of Goodfellow *et al.* proposed in [13]. The loss function for optimizing D has been defined in Eq(10).

4. Training of Multi-rate ℓ_∞ -CNN

In this section, we present the details of training the proposed ℓ_∞ -CNN for near-lossless image decompression, including how to train the ℓ_∞ -CNN for multiple compression bit rates so that it becomes universal and applicable on a wide range of bit rates (compression ratios).

4.1. Dataset

In the existing works on CNN-based compression artifacts removal [15, 12, 10], data used for training are from

the popular datasets like BSD100, ImageNet or MSCOCO. However, because images in these datasets are already compressed and have relatively low resolutions, they are not suitable as the ground truth for our purpose of ultra high fidelity image compression for professional applications. Instead we choose the high-quality image dataset DIV2K for training. The DIV2K dataset is a newly proposed 2K resolution image dataset for image restoration tasks. In the collaborative compression phase, we adopt the ℓ_∞ -constrained (or near-lossless) CALIC [30] to guarantee the compression error to be no larger than a specified bound τ for every pixel ($\tau = 6, 8, 10, 12, 14$ used in our experiments).

4.2. Training Details

Images in the DIV2K dataset are decomposed into 64×64 sub-images with stride 32, after compressed by the near-lossless CALIC algorithm. In the training phase, we train our networks using Adam optimizer with momentum term $\beta_1 = 0.9$. The neural networks are trained with 100 epochs at the learning rate of 10^{-4} and other 50 epochs with learning rate of 10^{-5} . To ensure the stability of the adversarial training, we perform the one-sided label smoothing for the discriminative network D proposed in [25]. It is noteworthy that we initialize the proposed ℓ_∞ -CNN without adversarial loss in the first 50 epochs. The reason is, at the early stage of training, images reconstructed by ℓ_∞ -CNN can be distinguished easily by discriminator D . It is unnecessary to feed the reconstructed images to discriminator D at the early stage.

4.3. Multi-rate Training

In previous CNN-based methods for compression artifacts removal, the training is carried out only with respect to a single compression rate [10, 15, 12]. That is, the training images are all of the same quality factor (QF) of the JPEG compression standard. Needless to say, the CNN learned for a given QF may not work well for images compressed in different QF's. Alternatively, many QF-specific CNNs can be trained for different QF's, but this approach is inefficient in practice. In this work, we train a unified ℓ_∞ -CNN for restoring images compressed in a range of bit rates. Each image in the training set is compressed for different, from low to high compression ratios, or for increasing ℓ_∞ bounds $\tau = 6, \dots, 14$. Thus, each patch in the original image has multiple compressed versions of different qualities, forming multiple sample pairs; all of them participate in the training of the multi-rate ℓ_∞ -CNN. It turns out, as shown in the following section, that the resulting multi-rate ℓ_∞ -CNN is more robust than the single-rate counterpart. The multi-rate ℓ_∞ -CNN even outperforms the single-rate ℓ_∞ -CNN on testing images that are compressed at the said single rate.

5. Performance Evaluation

5.1. Objective Evaluation

We have implemented the proposed ℓ_∞ -CNN for the task of removing compression artifacts, and conducted extensive experiments of near-lossless image decompression with it. In this section, we compare our results with two popular image compression algorithms: JPEG 2000 [27] and WebP [14]. Webp is an image format developed by Google, announced in 2010 as a new open standard for image compression. To compare fairly, for each test image, the rates of JPEG2000 and WebP are adjusted to match that of the near-lossless CALIC.

In addition, we also compare the new ℓ_∞ -CNN with ARCNN after training the latter with our dataset. Unfortunately, we cannot compare with other CNN-based methods for compression artifacts removal because of no access to the authors' source codes. In order to isolate the effects of imposing the ℓ_∞ error bounds, we also train two baselines in multi-rate mode using our network architecture, and compare the two baselines with the multi-rate ℓ_∞ -CNN. One of the baselines is trained using only the MSE loss, and another is trained using MSE loss and adversarial loss.

Three commonly used datasets LIVE1, Set14 and BSD100 are used to evaluate the above mentioned methods. In addition, we add a set of high-resolution aerial and satellite images as test images, for they are typical of those in professional applications.

Performance results of the competing methods are tabulated in Tables 1, 2, 3 and 4. As demonstrated in Tables 1, 2, 3 and 4, the ℓ_∞ -CNN outperforms JPEG2000, WebP and ARCNN consistently. As expected, the baseline model trained using only the MSE loss achieves the highest PSNR. However, remarkably, after adding the ℓ_∞ fidelity criterion, the ℓ_∞ -CNN achieves a much tighter ℓ_∞ bound without materially affecting the ℓ_2 error.

Finally, we would like to bring readers' attention to the enlarged parts of Figure 5 and 6. In the red window of Figure 5, the original image has a rectangular structure that is severely degraded by the near-lossless CALIC, and completely removed by JPEG 2000 and WebP. ARCNN fails to repair the degradation of CALIC and only makes the image more blurred. In contrast, the proposed ℓ_∞ -CNN is able to recover the original structure from the poor near-lossless CALIC decompressed image. In the blue window of Figure 5, the lines are jagged in the near-lossless CALIC and WebP images, and almost erased in the JPEG 2000 image. Here ARCNN fails to remove the jaggy artifacts and further blurs the lines. Only the ℓ_∞ -CNN is able to recover the lines faithfully.

In the red and blue windows of Figure 6, the sharp dent structures are visibly distorted by near-lossless CALIC, and they are made smaller and smoother by JPEG 2000 and

Table 1. Comparisons with the state-of-the-art methods on the set of aerial and satellite images.

τ	Measure	CALIC	JPEG2000	WebP	ARCNN	ℓ_∞ -CNN single-rate	MSE + GAN	MSE	ℓ_∞ -CNN multi-rate
$\tau=6$	PSNR	37.35	38.35	38.23	38.37	39.21	38.81	39.60	39.51
	SSIM	0.9411	0.9487	0.9538	0.9516	0.9601	0.9481	0.9620	0.9614
	ℓ_∞ bound	6	18.32	18.34	11.24	7.24	11.39	11.25	6.95
$\tau=8$	PSNR	35.15	36.91	36.72	36.96	37.49	37.31	37.84	37.76
	SSIM	0.9131	0.9327	0.9376	0.9378	0.9432	0.9347	0.9462	0.9456
	ℓ_∞ bound	8	25.05	23.59	15.05	9.73	15.01	14.89	9.24
$\tau=10$	PSNR	33.49	35.68	35.56	35.61	36.12	35.98	36.39	36.30
	SSIM	0.8880	0.9159	0.9213	0.9199	0.9268	0.9164	0.9293	0.9285
	ℓ_∞ bound	10	28.09	27.14	18.36	12.16	18.14	18.05	11.87
$\tau=12$	PSNR	32.16	34.78	34.54	34.44	34.94	34.84	35.18	35.11
	SSIM	0.8644	0.9008	0.9047	0.9023	0.9097	0.8960	0.9119	0.9112
	ℓ_∞ bound	12	34.91	32.64	21.22	14.56	20.94	20.58	14.18
$\tau=14$	PSNR	31.05	33.94	33.72	33.38	33.90	33.81	34.16	34.02
	SSIM	0.8431	0.8852	0.8890	0.8832	0.8912	0.8831	0.8942	0.8931
	ℓ_∞ bound	14	41.05	39.60	24.32	16.58	24.15	24.01	16.23

Table 2. Comparisons with the state-of-the-art methods on dataset LIVE1.

τ	Measure	CALIC	JPEG2000	WebP	ARCNN	ℓ_∞ -CNN single-rate	MSE + GAN	MSE	ℓ_∞ -CNN multi-rate
$\tau=6$	PSNR	37.13	38.32	38.11	38.05	39.01	38.69	39.61	39.45
	SSIM	0.9503	0.9623	0.9668	0.9627	0.9702	0.9567	0.9731	0.9721
	ℓ_∞ Bound	6	20.66	19.10	11.83	7.81	11.85	11.79	7.54
$\tau=8$	PSNR	35.05	36.62	36.55	36.65	37.31	37.13	37.84	37.69
	SSIM	0.9299	0.9496	0.9563	0.9546	0.9597	0.9483	0.9632	0.9621
	ℓ_∞ bound	8	26.34	24.28	15.86	10.81	15.56	15.37	10.34
$\tau=10$	PSNR	33.21	35.23	35.21	35.02	35.87	35.85	36.38	36.22
	SSIM	0.9108	0.9359	0.9449	0.9407	0.9485	0.9398	0.9518	0.9512
	ℓ_∞ bound	10	31.41	29.17	19.34	12.63	18.91	18.61	12.21
$\tau=12$	PSNR	31.80	34.26	34.21	33.83	34.69	34.63	35.17	35.00
	SSIM	0.8909	0.9237	0.9338	0.9271	0.9368	0.9254	0.9402	0.9389
	ℓ_∞ bound	12	36.65	34.03	22.24	14.88	21.88	21.54	14.54
$\tau=14$	PSNR	30.62	33.42	33.35	32.76	33.67	33.61	34.17	33.95
	SSIM	0.8721	0.9123	0.9231	0.9119	0.9232	0.9105	0.9274	0.9266
	ℓ_∞ bound	14	43.37	40.03	26.06	17.08	25.73	24.91	16.71

WebP; these compression distortions can lead to misjudgments of the size, depth, and shape of these structures on the ground. While ARCNN does not cure these problems but again blurs the image, the proposed image recovers the ground truth flawlessly.

6. Conclusion

In this paper, we identify a serious weakness of the existing CNN-based techniques for compression artifacts removal, and propose to incorporate an ℓ_∞ fidelity term in the design of network to preserve small, distinctive details of

Table 3. Comparisons with the state-of-the-art methods on datasets Set14.

τ	Measure	CALIC	JPEG2000	WebP	ARCNN	ℓ_∞ -CNN single-rate	MSE + GAN	MSE	ℓ_∞ -CNN multi-rate
$\tau=6$	PSNR	37.15	37.76	37.90	37.95	38.78	38.41	39.20	39.05
	SSIM	0.9497	0.9561	0.9644	0.9596	0.9660	0.9548	0.9682	0.9675
	ℓ_∞ bound	6	22.21	19.93	11.50	7.62	11.64	11.54	7.37
$\tau=8$	PSNR	35.01	36.28	36.38	36.59	37.21	36.96	37.60	37.46
	SSIM	0.9242	0.9426	0.9520	0.9478	0.9521	0.9421	0.9554	0.9546
	ℓ_∞ bound	8	27.10	23.57	15.64	10.31	15.27	15.18	10.05
$\tau=10$	PSNR	33.34	35.01	35.13	35.08	35.84	35.76	36.20	36.11
	SSIM	0.9029	0.9290	0.9398	0.9314	0.9392	0.9312	0.9438	0.9428
	ℓ_∞ bound	10	30.64	28.71	19.14	12.46	18.76	18.51	12.13
$\tau=12$	PSNR	31.95	34.16	34.15	34.01	34.85	34.85	35.14	35.01
	SSIM	0.8793	0.9183	0.9282	0.9172	0.9270	0.9154	0.9315	0.9305
	ℓ_∞ bound	12	36.04	32.57	21.71	14.67	21.83	21.64	14.24
$\tau=14$	PSNR	30.73	33.34	33.35	32.96	33.79	33.71	34.06	33.94
	SSIM	0.8583	0.9053	0.9160	0.9011	0.9119	0.9004	0.9167	0.9160
	ℓ_∞ bound	14	42.35	40.07	25.35	16.64	24.86	24.42	16.32

Table 4. Comparisons with the state-of-the-art methods on dataset BSD100.

τ	Measure	CALIC	JPEG2000	WebP	ARCNN	ℓ_∞ -CNN single-rate	MSE + GAN	MSE	ℓ_∞ -CNN multi-rate
$\tau=6$	PSNR	37.08	37.79	37.87	38.05	38.80	38.45	39.25	39.12
	SSIM	0.9548	0.9622	0.9688	0.9658	0.9714	0.9623	0.9740	0.9730
	ℓ_∞ bound	6	20.21	18.49	11.73	7.51	11.28	11.14	7.19
$\tau=8$	PSNR	34.81	36.07	36.15	36.37	36.91	36.75	37.36	37.21
	SSIM	0.9339	0.9474	0.9563	9.9560	0.9594	0.9512	0.9619	0.9612
	ℓ_∞ bound	8	25.20	23.61	15.73	10.24	15.09	14.78	9.87
$\tau=10$	PSNR	33.07	34.73	34.79	34.89	35.60	35.52	35.88	35.75
	SSIM	0.9119	0.9328	0.9431	0.9405	0.9468	0.9386	0.9486	0.9479
	ℓ_∞ bound	10	29.69	28.61	19.15	12.51	18.94	18.58	12.14
$\tau=12$	PSNR	31.70	33.75	33.74	33.67	34.28	34.15	34.61	34.50
	SSIM	0.8934	0.9193	0.9303	0.9257	0.9312	0.9241	0.9354	0.9347
	ℓ_∞ bound	12	35.10	32.67	22.05	14.56	21.65	21.23	14.48
$\tau=14$	PSNR	30.50	32.92	32.89	32.67	33.31	33.24	33.61	33.50
	SSIM	0.8728	0.9066	0.9181	0.9102	0.9176	0.9100	0.9213	0.9208
	ℓ_∞ bound	14	41.31	38.04	26.10	16.88	25.40	25.12	16.84

the original image. Experimental results show that the proposed ℓ_∞ -CNN outperforms the state-of-the-art methods in ℓ_∞ error metric and perceptual quality, while being competitive in ℓ_2 error metric as well. This research ushers in a new neural network paradigm of ultra high fidelity image compression that is ideally suited for applications of preci-

sion machine vision in the professional fields of medicine, space, engineering and sciences.

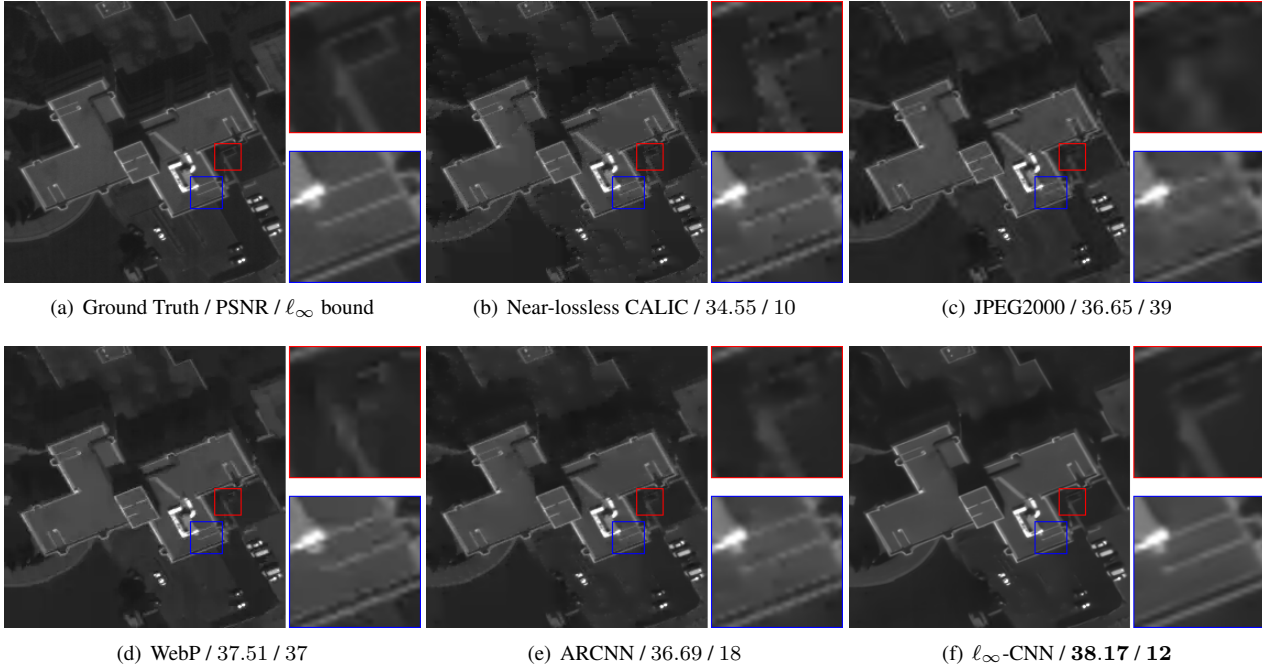


Figure 5. Comparisons with the state-of-the-art methods on an aerial image.

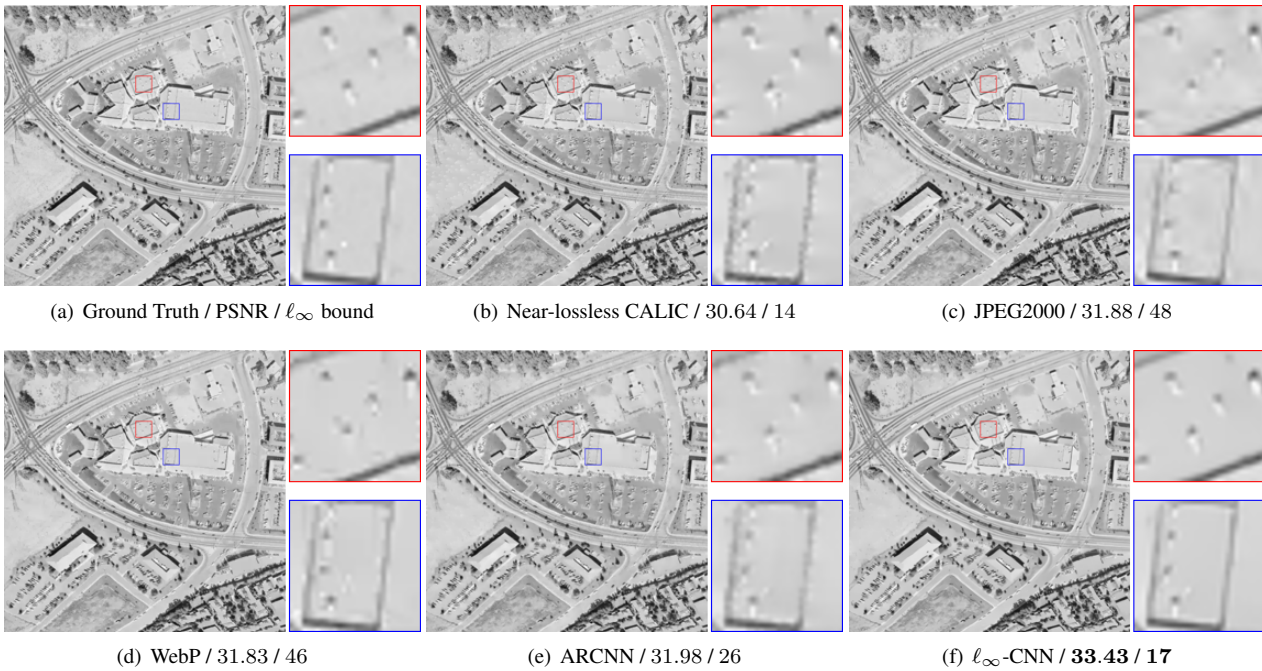


Figure 6. Comparisons with the state-of-the-art methods on an aerial image.

References

- [1] F. Alter, S. Durand, and J. Froment. Adapted total variation for artifact free decompression of jpeg images. *Journal of Mathematical Imaging and Vision*, 23(2):199–211, 2005.
- [2] I. Avcibas, N. Memon, B. Sankur, and K. Sayood. A progressive lossless/near-lossless image compression algorithm. *IEEE Signal Processing Letters*, 9(10):312–314, 2002.
- [3] N. V. Boulgouris, D. Tzovaras, and M. G. Strintzis. Lossless image compression based on optimal prediction, adaptive lifting, and conditional arithmetic coding. *IEEE Transactions on Image Processing*, 10(1):1–14, 2001.
- [4] K. Bredies and M. Holler. A total variation–based jpeg de-

- compression model. *SIAM Journal on Imaging Sciences*, 5(1):366–393, 2012.
- [5] A. R. Calderbank, I. Daubechies, W. Sweldens, and B.-L. Yeo. Lossless image compression using integer to integer wavelet transforms. In *Image Processing, 1997. Proceedings., International Conference on*, volume 1, pages 596–599. IEEE, 1997.
- [6] H. Chang, M. K. Ng, and T. Zeng. Reducing artifacts in jpeg decompression via a learned dictionary. *IEEE transactions on signal processing*, 62(3):718–728, 2014.
- [7] K. Chen and T. V. Ramabadran. Near-lossless compression of medical images through entropy-coded dpcm. *IEEE Transactions on Medical Imaging*, 13(3):538–548, 1994.
- [8] Y. Dar, A. M. Bruckstein, M. Elad, and R. Giryes. Post-processing of compressed images via sequential denoising. *IEEE Transactions on Image Processing*, 25(7):3044–3058, 2016.
- [9] E. L. Denton, S. Chintala, R. Fergus, et al. Deep generative image models using a laplacian pyramid of adversarial networks. In *Advances in neural information processing systems*, pages 1486–1494, 2015.
- [10] C. Dong, Y. Deng, C. Change Loy, and X. Tang. Compression artifacts reduction by a deep convolutional network. In *Proceedings of the IEEE International Conference on Computer Vision*, pages 576–584, 2015.
- [11] A. Foi, V. Katkovnik, and K. Egiazarian. Pointwise shape-adaptive dct for high-quality denoising and deblocking of grayscale and color images. *IEEE Transactions on Image Processing*, 16(5):1395–1411, 2007.
- [12] L. Galteri, L. Seidenari, M. Bertini, and A. Del Bimbo. Deep generative adversarial compression artifact removal. *arXiv preprint arXiv:1704.02518*, 2017.
- [13] I. Goodfellow, J. Pouget-Abadie, M. Mirza, B. Xu, D. Warde-Farley, S. Ozair, A. Courville, and Y. Bengio. Generative adversarial nets. In *Advances in neural information processing systems*, pages 2672–2680, 2014.
- [14] Google. A new image format for the web. <https://developers.google.com/speed/webp/>.
- [15] J. Guo and H. Chao. One-to-many network for visually pleasing compression artifacts reduction. *arXiv preprint arXiv:1611.04994*, 2016.
- [16] K. He, X. Zhang, S. Ren, and J. Sun. Deep residual learning for image recognition. In *Proceedings of the IEEE conference on computer vision and pattern recognition*, pages 770–778, 2016.
- [17] L. Ke and M. W. Marcellin. Near-lossless image compression: minimum-entropy, constrained-error dpcm. *IEEE Transactions on Image Processing*, 7(2):225–228, 1998.
- [18] C. Ledig, L. Theis, F. Huszár, J. Caballero, A. Cunningham, A. Acosta, A. Aitken, A. Tejani, J. Totz, Z. Wang, et al. Photo-realistic single image super-resolution using a generative adversarial network. *arXiv preprint arXiv:1609.04802*, 2016.
- [19] Y. Li, F. Guo, R. T. Tan, and M. S. Brown. A contrast enhancement framework with jpeg artifacts suppression. In *European Conference on Computer Vision*, pages 174–188. Springer, 2014.
- [20] X. Liu, X. Wu, J. Zhou, and D. Zhao. Data-driven soft decoding of compressed images in dual transform-pixel domain. *IEEE Transactions on Image Processing*, 25(4):1649–1659, 2016.
- [21] S. Maniccam and N. G. Bourbakis. Lossless image compression and encryption using scan. *Pattern Recognition*, 34(6):1229–1245, 2001.
- [22] A. Radford, L. Metz, and S. Chintala. Unsupervised representation learning with deep convolutional generative adversarial networks. *arXiv preprint arXiv:1511.06434*, 2015.
- [23] S. Reed, Z. Akata, X. Yan, L. Logeswaran, B. Schiele, and H. Lee. Generative adversarial text to image synthesis. *arXiv preprint arXiv:1605.05396*, 2016.
- [24] H. C. Reeve and J. S. Lim. Reduction of blocking effects in image coding. *Optical Engineering*, 23(1):230134, 1984.
- [25] T. Salimans, I. Goodfellow, W. Zaremba, V. Cheung, A. Radford, and X. Chen. Improved techniques for training gans. In *Advances in Neural Information Processing Systems*, pages 2234–2242, 2016.
- [26] K. Simonyan and A. Zisserman. Very deep convolutional networks for large-scale image recognition. *arXiv preprint arXiv:1409.1556*, 2014.
- [27] A. Skodras, C. Christopoulos, and T. Ebrahimi. The jpeg 2000 still image compression standard. *IEEE Signal processing magazine*, 18(5):36–58, 2001.
- [28] P. Svoboda, M. Hradis, D. Barina, and P. Zemcik. Compression artifacts removal using convolutional neural networks. *arXiv preprint arXiv:1605.00366*, 2016.
- [29] C. Szegedy, W. Liu, Y. Jia, P. Sermanet, S. Reed, D. Anguelov, D. Erhan, V. Vanhoucke, and A. Rabinovich. Going deeper with convolutions. In *Proceedings of the IEEE conference on computer vision and pattern recognition*, pages 1–9, 2015.
- [30] X. Wu, W. K. Choi, and P. Bao. L_∞ constrained high-fidelity image compression via adaptive context modeling. In *Data Compression Conference, 1997. DCC'97. Proceedings*, pages 91–100. IEEE, 1997.
- [31] X. Wu and N. Memon. Calic-a context based adaptive lossless image codec. In *Acoustics, Speech, and Signal Processing, 1996. ICASSP-96. Conference Proceedings., 1996 IEEE International Conference on*, volume 4, pages 1890–1893. IEEE, 1996.
- [32] G. Zhai, W. Zhang, X. Yang, W. Lin, and Y. Xu. Efficient image deblocking based on postfiltering in shifted windows. *IEEE Transactions on Circuits and Systems for Video Technology*, 18(1):122–126, 2008.
- [33] X. Zhang, R. Xiong, X. Fan, S. Ma, and W. Gao. Compression artifact reduction by overlapped-block transform coefficient estimation with block similarity. *IEEE transactions on image processing*, 22(12):4613–4626, 2013.
- [34] J.-Y. Zhu, T. Park, P. Isola, and A. A. Efros. Unpaired image-to-image translation using cycle-consistent adversarial networks. *arXiv preprint arXiv:1703.10593*, 2017.